

Novel Lanthanide Luminescent Materials Based on Complexes of 3-Hydroxypicolinic Acid and Silica Nanoparticles

Paula C. R. Soares-Santos,[†] Helena I. S. Nogueira,[†] Vitor Félix,[†]
Michael G. B. Drew,[§] Rute A. Sá Ferreira,[‡] Luís D. Carlos,^{*,‡} and
Tito Trindade^{*,†}

Departments of Chemistry and Physics, University of Aveiro,
CICECO, 3810-193 Aveiro, Portugal, and Department of Chemistry,
University of Reading, Whiteknights, Reading UK RG6 6AD

Received April 15, 2002. Revised Manuscript Received October 9, 2002

New lanthanide complexes of 3-hydroxypicolinic acid (HpicOH) were prepared: $[\text{Ln}(\text{H}_2\text{O})(\text{picOH})_2(\mu\text{-HpicO})]\cdot 3\text{H}_2\text{O}$ (Ln = Eu, Tb, Er). The complexes were characterized using photoluminescence, infrared, Raman, and ^1H NMR spectroscopy, and elemental analysis. The crystal structure of $[\text{Eu}(\text{H}_2\text{O})(\text{picOH})_2(\mu\text{-HpicO})]\cdot 3\text{H}_2\text{O}$ **1** was determined by X-ray diffraction. Compound **1** crystallizes in a monoclinic system with space group $P2_1/c$ and cell parameters $a = 9.105(13)$ Å, $b = 18.796(25)$ Å, and $c = 13.531(17)$ Å, and $\beta = 104.86(1)$ deg. The 3-hydroxypicolinate ligands coordinate through both N,O - or O,O -chelation to the lanthanide ions, as shown by X-ray and spectroscopic results. Photoluminescence measurements were performed for the Eu(III) and Tb(III) complexes; the Eu(III) complex was investigated in more detail. The Eu(III) compound is highly luminescent and acts as a photoactive center in nanocomposite materials whose host matrixes are silica nanoparticles.

Introduction

In recent years there has been intense research on the synthesis of photoactive lanthanide complexes.^{1–3} The possibility of having ligands in such species that function as light-harvesting units has been investigated. These units can act as antennas for collecting light and transferring the energy to the lanthanide, originating extensive photoluminescence.⁴ Coordination compounds of this type may be regarded as photoactive units to fabricate novel optical materials, namely as luminescent centers in host matrixes.

Trivalent lanthanide ions form stable coordination complexes with a variety of organic ligands.^{5,6} Lanthanide complexes with ligands containing nitrogen and oxygen donors have been investigated (ethylenediaminetetraacetate and its derivatives⁵ are good ex-

amples), in particular for aromatic ligands such as picolinate,⁷ dipicolinates,^{8–10} 2,2'-bipyridine-6,6'-dicarboxylic acid¹¹ and bis-pyridones,¹² to mention just a few. The latter constitute a very interesting type of complexes, because energy transfer from the aromatic groups close to the lanthanide ions may considerably enhance the luminescence efficiency of the ion. For example, it has been reported that Tb(III) luminescence is enhanced more than 10^4 -fold by dipicolinic acid.^{9,10} The ligand 3-hydroxypicolinic acid (HpicOH), used in the present work, is a potential chelate with interesting possibilities, such as N,O -chelation (of the monodeprotonated ligand, picOH^- , through the pyridinic nitrogen and the carboxylate group, forming a five-membered chelate ring) or O,O -chelation (through the carboxylate group and the deprotonated hydroxyl group, forming a six-membered chelate ring; either of the twice deprotonated ligand, picO^{2-} , or, as found in this work, of the monodeprotonated HpicO⁻ ligand with a protonated pyridinic nitrogen) as shown in Scheme 1.

Here, the synthesis of the lanthanide complexes $[\text{Ln}(\text{H}_2\text{O})(\text{picOH})_2(\mu\text{-HpicO})]\cdot 3\text{H}_2\text{O}$ (Ln = Eu **1**, Tb **2**, Er **3**) is reported with their characterization using vibrational and NMR spectroscopies. The chelation modes of

* Authors to whom correspondence should be addressed. Dr. Luis António Dias Carlos: phone 351-234-370946; fax 351-234-424965, e-mail lcarlos@fis.ua.pt. Dr. Tito Trindade: phone 351-234-370726; fax 351-234-370084; e-mail ttrindade@dq.ua.pt.

[†] Department of Chemistry, University of Aveiro.

[‡] Department of Physics, University of Aveiro.

[§] University of Reading.

(1) Arnaud, N.; Vaquer, E.; Georges, J. *The Analyst* **1998**, *123*, 261.

(2) Sá, G. F.; Malta, O. L.; Donegá, C. M.; Simas, A. M.; Longo R. L.; Santa-Cruz, P. A.; Silva, E. F., Jr. *Coord. Chem. Rev.* **2000**, *196*, 165.

(3) Vicentini, G.; Zinner, L. B.; Zukerman-Schpector, J.; Zinner, K. *Coord. Chem. Rev.* **2000**, *196*, 353.

(4) Lianshe, F.; Qingguo, M.; Hongjie, Z.; Shubin, W.; Kuiyue, Y.; Jiazuan, N. *J. Phys. Chem. Solids* **2000**, *61*, 1877.

(5) Hart, F. A. Scandium, Yttrium and the Lanthanides. In *Comprehensive Coordination Chemistry*, Wilkinson, G., Gillard, R. D., McCleverty, J. A., Eds.; Pergamon Press: Elmsford, NY, 1987; Vol. 3, p 1059.

(6) Parker, D.; Williams, J. A. G. *J. Chem. Soc., Dalton Trans.* **1996**, 3613.

(7) Park, Y. J.; Lee, B. H.; Kim, W. H.; Do, Y. *J. Colloid Interface Sci.* **1999**, *209*, 268.

(8) Albertsson, J. *Acta Chem. Scand.* **1970**, *24*, 1213.

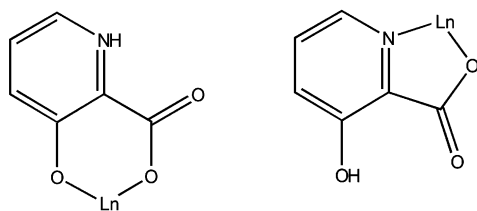
(9) Barela, T. D.; Sherry, A. D. *Anal. Biochem.* **1976**, *71*, 351.

(10) Lamture, J. B.; Zhou, Z. H.; Kumar, A. S.; Wensel, T. G. *Inorg. Chem.* **1995**, *34*, 864.

(11) Bünzli, J. G.; Charbonnière, L. J.; Ziessel, R. F. *J. Chem. Soc., Dalton Trans.* **2000**, 1917.

(12) Goodgame, D. M. L.; Hill, S. P. W.; Smith, A. M.; Williams, D. *J. Chem. Soc., Dalton Trans.* **1994**, 859.

Scheme 1

O,O-chelation (HpicO⁻ ligand) N,O-chelation (picOH⁻ ligand)

the ligand to the different lanthanides is discussed on the basis of the X-ray crystal structure of [Eu(H₂O)(picOH)₂(μ-HpicO)]·3H₂O **1** and spectroscopic results, and compared to published data for analogous compounds of *d*-transition metals.^{13–16} The 3-hydroxypicolinate ligands show both *N,O*- and *O,O*-chelation in the crystal structure of the Eu(III) complex **1**; spectroscopic data are consistent with the Tb(III) and Er(III) complexes, **2** and **3** respectively, having the same type of coordination. The local environment of the lanthanide ions in these compounds is further discussed on the basis of their luminescence properties.

There has been great interest in developing luminescent nanomaterials for applications in the optoelectronic^{17,18} and biodetection fields.¹⁹ Size-tuned semiconducting nanocrystals (e.g., II/VI semiconductors) have been investigated in some detail.^{17–20} The strategy reported here involves using another type of material to fabricate novel luminescent nanomaterials via a low-temperature processing method. In fact, it was found that the Eu(III) complex **1** is easily dispersed in a silica network. Nanoparticles of 1/SiO₂ were prepared by a sol–gel method. For the Eu(III) complex **1** and the hybrid derivative 1/SiO₂, a detailed analysis on the luminescence properties was carried out and is presented here.

Experimental Section

All chemicals were supplied by Aldrich and used as received.

Preparation of [Ln(H₂O)(picOH)₂(μ-HpicO)]·3H₂O (Ln = Eu **1, Tb **2**, Er **3**).** Ln(OH)₃ (Ln = Eu, Tb, Er) starting compounds were prepared by adding aqueous solutions (8 mL) of KOH (4.5 mmol) to an equal volume of aqueous solutions containing the lanthanide chloride salt (1.5 mmol). The solid formed was stirred over 90 min, filtered, and washed thoroughly with distilled water.

The 3-hydroxypicolinate lanthanide complexes were prepared similarly. Typically, 1 mmol of Ln(OH)₃ was added to an aqueous solution (25 mL) containing 3-hydroxypicolinic acid (4 mmol). This mixture was stirred during 1 h, then heated for 30 min at 80 °C, and further stirred over 8 h at room

temperature. The solid obtained was filtered, washed thoroughly with distilled water, and dried over silica gel. Single crystals of [Eu(H₂O)(picOH)₂(μ-HpicO)]·3H₂O **1** were obtained from the filtrate after slow evaporation for two months.

Preparation of SiO₂ Nanocomposites. The Eu(III) complex **1** was dispersed within a silica matrix using a sol–gel method adapted from the Stöber method.²¹

Tetraethoxysilane (TEOS, 0.32 mL) was added to 1 mL of absolute ethanol, followed by the addition of a DMSO solution (0.33 mL) containing complex **1** (10.5 mg). The alkoxide hydrolysis was promoted by addition of 2 mL of distilled water to the previous solution. This mixture was allowed to stand over a few days until a rigid gel was formed. The gel was then dried in an oven at 60 °C leading to solid pieces of a 1/SiO₂ composite material (Eu/SiO₂ composite **A**).

When the alkoxide hydrolysis was catalyzed by adding a NH₄OH solution (25%) instead of water, nanoparticles of the 1/SiO₂ composite material (Eu/SiO₂ composite **B**) were obtained. TEOS (0.78 mL) was added to a mixture of absolute ethanol (5 mL) and distilled water (0.06 g). This mixture was allowed to stand over 30 min followed by the addition of a DMSO solution (2 mL) containing complex **1** (27.9 mg); finally, 2 mL of NH₄OH solution (25%) was added. On standing for 30 min, the colloid was filtered and washed thoroughly with distilled water (Eu/SiO₂ composite **B**).

Instrumentation. Infrared spectra were measured as KBr disks using a Mattson 7000 FT instrument. Raman spectra were recorded using a Brüker RFS100/S FT-Raman spectrometer (Nd:YAG laser, 1064 nm excitation). ¹H NMR spectra were recorded using a Brüker AMX300 spectrometer (¹H, 300 MHz; ¹³C, 75.4 MHz) referenced to Si(CH₃)₄ or the solvent. Microanalyses (C, H, and N) were measured in the Department of Chemistry, University of Aveiro, and the lanthanide content in the complexes was measured by ICP (Analytical Laboratories, University of Aveiro).

Room-temperature photoluminescence spectra were recorded on a Jobin Yvon-Spex spectrometer (HR 460) coupled to a R928 Hamamatsu photomultiplier. An He–Cd laser beam (325 nm and P = 30 mW) and a 150 W Xe arc lamp coupled to an excitation monochromator Jobin Yvon - Spex (TRIAX 180) were used as excitation sources. All the spectra were corrected for the response of the detector. The lifetime measurements were carried out using a pulsed Xe arc lamp (5 mJ/pulse, 3 μs bandwidth) coupled to a Kratos GM-252 monochromator and a Spex 1934 C phosphorimeter.

The X-ray powder diffraction (XRD) patterns were recorded using a Philips instrument operating with Cu Kα radiation (λ = 1.54178 Å) at 40 kV/50 mA. Scanning electron microscopy (SEM) images were obtained using a FEG-SEM Hitachi S4100 microscope operating at 25 kV. The samples were prepared by deposition of an aliquot of an ethanol suspension of the sample on aluminum pieces and then coated with evaporated carbon.

Crystallography. Single crystals of **1** were obtained by slow evaporation from an aqueous solution of the complex at room temperature. The crystal data and refinement details are given in Table 1.

X-ray data were measured using MAR research image plate system using a graphite-monochromated Mo Kα radiation (λ = 0.71073 Å) at ≈295 K. The selected crystal mounted in a glass capillary under saturated solvent atmosphere was positioned at 70 mm from the plate. In total, 95 frames were taken at 2° intervals using a counting time adequate to the crystal diffraction pattern. Data analysis was performed with the XDS program.²² An empirical absorption correction was applied to intensities of **1**, using a version of the DIFABS program modified for image plate geometry.²³

Intensities of 5766 observations were collected, of which 3243 were independent reflections giving a *R*_{int} of 0.0290. The

(13) Quintal, S. M. O.; Nogueira, H. I. S.; Félix, V.; Drew, M. G. B. *New J. Chem.* **2000**, *24*, 511.

(14) Quintal, S. M. O.; Nogueira, H. I. S.; Carapuça, H. M.; Félix, V.; Drew, M. G. B. *J. Chem. Soc., Dalton Trans.* **2001**, 3196.

(15) Griffith, W. P.; Nogueira, H. I. S.; Parkin, B. C.; Sheppard, R. N.; White, A. J. P.; Williams, D. J. *J. Chem. Soc., Dalton Trans.* **1995**, 1775.

(16) Edwards, C. F.; Griffith, W. P.; White, A. J. P.; Williams, D. J. *J. Chem. Soc., Dalton Trans.* **1993**, 3813.

(17) Nirmal, M.; Dabbousi, B. O.; Bawendi, M. G.; Macklin, J. J.; Trautman, J. K.; Harris, T. D.; Brus, L. E. *Nature* **1996**, *383*, 802.

(18) Klein, D. L.; Roth, R.; Lim, A. K. L.; Alivisatos, A. P.; McEuen, P. L. *Nature* **1997**, *389*, 699.

(19) Bruchez, M., Jr.; Moronne, M.; Gin, P.; Weiss, S.; Alivisatos, A. P. *Science* **1998**, *281*, 2013.

(20) Trindade, T.; O'Brien, P.; Pickett, N. L. *Chem. Mater.* **2001**, *13*, 3843.

(21) Stöber, W.; Fink, A.; Bohn, E. *J. Colloid Interface Sci.* **1968**, *26*, 62.

(22) Kabsch, W. *J. Appl. Crystallogr.* **1988**, *21*, 916.

(23) Walker, N.; Stuart, D. *DIFABS, Acta Crystallogr., Sect. A* **1983**, *39*, 158.

Table 1. Crystallographic Data for [Eu(picOH)₃(H₂O)]·3H₂O **1**

formula	C ₁₈ H ₂₀ EuN ₃ O ₁₃
<i>M</i>	638.33
crystal system	monoclinic
space group	<i>P</i> 2 ₁ / <i>c</i>
<i>a</i> (Å)	9.105(13)
<i>b</i> (Å)	18.796(25)
<i>c</i> (Å)	13.531(17)
β (deg)	104.86(1)
<i>V</i> /Å ³	2238(5)
<i>Z</i>	4
<i>D</i> _{calcd} /gcm ⁻³	1.894
μ (mm ⁻¹)	2.877
<i>F</i> (000)	1264
final <i>R</i> indices [<i>I</i> > 2σ(<i>I</i>)]	
<i>R</i> ₁ and <i>wR</i> ₂ ^a	0.0348, 0.0906
<i>R</i> indices (all data)	
<i>R</i> ₁ and <i>wR</i> ₂	0.0483, 0.0978

^a $R_1 = \sum(\Delta F)/\sum(F_o)$, $wR_2 = \{\sum[w\Delta(F^2)^2]/\sum[w(F_o^2)^2]\}^{1/2}$, $w = 1/[\sigma^2(F_o^2) + (0.0528P) + 6.0222P]$, where $P = (\text{Max}(F_o^2, \theta) + 2F_c^2)/3$. This material is available free of charge via the Internet at <http://pubs.acs.org>.²

structure was solved by direct methods and subsequent difference Fourier syntheses, and refined by full-matrix least-squares refinement method on F^2 using the SHELX97 software package.²⁴ Anisotropic displacements were refined for all non-hydrogen atoms. Hydrogen atoms bonded to carbon atoms were introduced in the refinement at idealized geometric positions given thermal isotropic parameters equivalent to 1.2 times those of the atom to which they are attached. The positions of the hydrogen atoms of water molecules, of the two phenol groups, and as well as the pyridine N–H group, were discernible from difference Fourier maps. The first ones were introduced in the refinement assuming O–H distances and angles H–O–H constrained to 0.82 Å and 104.5°, respectively, whereas for the second ones only the restraint on the distance was applied. The N–H group was refined with a distance constrained to 0.89 Å. The thermal motion of these hydrogen atoms was described using individual thermal isotropic parameters. The final refinements of 352 parameters converged to *R*₁ and *wR*₂ values quoted in Table 1. The final residual electronic density in Δ*F* map, in the range 1.19 to -0.91 eÅ⁻³, was within the expected values. The ORTEP plot and crystal packing diagram were drawn with the PLATON program,²⁵ whereas the diagram of the polyhedra chain was performed using WEBLAB VIEWER software.²⁶

Results and Discussion

Preparation of Lanthanide(III) 3-Hydroxypicolinate Complexes. Suspensions of Ln(OH)₃ (Ln = Eu, Tb, Er) and HpicOH in aqueous solutions were stirred for 9 h to give a series of Ln complexes with the 3-hydroxypicolinate ligand. The solid product obtained from each preparation was filtered off and washed thoroughly with distilled water. Elemental analysis results (Table 4) are in accordance with the molecular formula [Ln(H₂O)(picOH)₂(μ-HpicO)]·3H₂O for all the complexes (Ln = Eu **1**, Tb **2**, Er **3**) as shown in the crystal structure of **1**, which is consistent with the spectroscopic data presented below.

Crystal Structure of [Eu(H₂O)(picOH)₂(μ-HpicO)]·3H₂O **1.** The asymmetric unit of **1** is composed of a [Eu(H₂O)(picOH)₂(μ-HpicO)] complex and three water

Table 2. Selected Bond Lengths (Å) and Angles (deg) for **1**

Eu–O(331)	2.309(4)	Eu–O(171)	2.373(4)
Eu–O(100)	2.389(4)	Eu–O(372) ^a	2.390(4)
Eu–O(371)	2.393(4)	Eu–O(271)	2.410(4)
Eu–N(21)	2.578(5)	Eu–N(11)	2.596(5)
O(331)–Eu–O(171)	123.7(2)	O(331)–Eu–O(100)	71.9(2)
O(171)–Eu–O(100)	136.0(2)	O(331)–Eu–O(372) ^a	143.4(1)
O(171)–Eu–O(372) ^a	78.8(2)	O(100)–Eu–O(372) ^a	72.4(1)
O(331)–Eu–O(371)	72.1(1)	O(171)–Eu–O(371)	77.7(2)
O(100)–Eu–O(371)	141.2(1)	O(372) ^a –Eu–O(371)	144.6(1)
O(331)–Eu–O(271)	137.0(2)	O(171)–Eu–O(271)	72.4(2)
O(100)–Eu–O(271)	127.3(2)	O(372) ^a –Eu–O(271)	73.8(1)
O(371)–Eu–O(271)	74.5(1)	O(331)–Eu–N(21)	86.0(2)
O(171)–Eu–N(21)	136.5(2)	O(100)–Eu–N(21)	80.3(2)
O(372) ^a –Eu–N(21)	95.7(2)	O(371)–Eu–N(21)	83.4(2)
O(271)–Eu–N(21)	64.3(1)	O(331)–Eu–N(11)	79.2(2)
O(171)–Eu–N(11)	64.7(2)	O(100)–Eu–N(11)	81.3(2)
O(372) ^a –Eu–N(11)	87.7(2)	O(371)–Eu–N(11)	105.5(2)
O(271)–Eu–N(11)	135.8(2)	N(21)–Eu–N(11)	159.3(2)
C(37) ^a –O(372) ^a –Eu	166.7(4)		

^a The following symmetry transformation is used to generate equivalent atoms: ^a*x*, -*y* + 3/2, *z* + 1/2.

molecules. Furthermore, the crystal displays a 1-D polymeric structure build-up from [Eu(H₂O)(picOH)₂]⁺ structural units linked by HpicO⁻ bridges which hold the europium centers at a long distance of 6.943(1) Å. An ORTEP view showing the atomic connectivities in the building block of the 1-D polymeric chain together with atomic notation scheme adopted is presented in Figure 1a, and the overall geometry of the polymeric chain with europium(III) centers drawn in the polyhedra mode is shown in Figure 1b. Selected bond lengths and angles in the metal coordination sphere are given in Table 2. All europium centers are bonded to two nitrogen and six oxygen atoms in a coordination environment that can be described as distorted triangulated dodecahedron (bisphenoid).²⁷ Two picOH⁻ ligands are almost trans making a dihedral angle of 9.1(1)° and display *N,O* coordination mode with Eu–N distances of 2.596(5) and 2.578(5) Å and Eu–O distances of 2.373(4) and 2.410(4) Å. The third HpicO⁻ ligand is coordinated by the oxygen atom of the phenol group and one oxygen atom from the carboxylate group in *O,O* chelation fashion with Eu–O distances of 2.393(4) and 2.309(4) Å. The coordination sphere of eight atoms is completed with one water molecule, with a Eu–O distance of 2.389(4) Å, and one oxygen atom of a carboxylate group from a second *O,O* chelated HpicO⁻ ligand belonging to the neighboring structural unit. This bridging oxygen is bonded almost linearly to the metal center with a Eu–O bond distance of 2.390(4) Å and a C–O–Eu angle of 166.7(4)°. From the Cambridge Crystallographic Data Base²⁸ we retrieved nineteen structures having EuN₂O₆ coordination polyhedra with Eu–N and Eu–O distances within a wider range of 2.448–2.655 Å and 2.224–2.510 Å, respectively.

The charge balance of the molecular formula for complex **1** requires that the three 3-hydroxypicolinate ligands are monoprotonated. Indeed, the final difference Fourier map revealed the unambiguous location of one hydrogen atom bonded to each of the two picOH⁻

(24) Sheldrick, G. M. *SHELXS-86*, *Acta Crystallogr., Sect. A* **1990**, *46*, 467; Sheldrick, G. M. *SHELX-97*, University of Göttingen, 1997.

(25) Spek, A. L. *PLATON, a Multipurpose Crystallographic Tool*; Utrecht University: Utrecht, The Netherlands, 1999.

(26) *WEBLAB VIEWER, version 2.01*; Molecular Simulations, Inc.: San Diego, CA, 1997.

(27) Wells, A. F. *Structural Inorganic Chemistry*; Clarendon Press: Oxford, 1984; pp 78 and 79.

(28) Allen, F. H.; Kennard, O. *Chem. Des. Autom. News* **1993**, *8*, 31.

Table 3. Dimensions of the Hydrogen Bonds

donor-H...acceptor	distances (Å)		angle (deg)
	H...A ^a	D...A ^a	D-H...A ^a
N(31)–H(31) ...O(372)	2.30(5)	2.665(5)	104(3)
N(31)–H(31) ...O(171)[<i>x</i> , 3/2 – <i>y</i> , –1/2 + <i>z</i>]	2.57(6)	3.035(7)	113(5)
N(31)–H(31) ...O(271)[<i>x</i> , 3/2 – <i>y</i> , –1/2 + <i>z</i>]	1.90(5)	2.779(6)	167(6)
O(100)–H(101) ...O(300)	1.89(2)	2.702(7)	172(7)
O(100)–H(102) ...O(200)	1.92(4)	2.712(6)	163(7)
O(131)–H(131) ...O(172)	1.77(10)	2.551(8)	160(11)
O(200)–H(201) ...O(272)[1 – <i>x</i> , 1/2 + <i>y</i> , 3/2 – <i>z</i>]	2.00(6)	2.811(7)	168(6)
O(200)–H(202) ...O(300)[1 – <i>x</i> , 2 – <i>y</i> , 2 – <i>z</i>]	1.99(6)	2.792(8)	167(6)
O(231)–H(231) ...O(272)	1.86(9)	2.610(7)	152(8)
O(300)–H(301) ...O(371)[<i>x</i> , 3/2 – <i>y</i> , 1/2 + <i>z</i>]	2.10(3)	2.892(5)	163(6)
O(300)–H(302) ...O(400)[<i>x</i> , 3/2 – <i>y</i> , –1/2 + <i>z</i>]	1.98(6)	2.778(10)	166(4)
O(400)–H(402) ...O(172)	1.89(9)	2.714(10)	173(11)

^a A and D denote the acceptors and donors, respectively.

Table 4. Analytical and Spectroscopic Data for Lanthanide Complexes of 3-Hydroxypicolinic Acid and the Free Ligand

compound	analysis ^a (%)				vibrational spectra ^b (cm ⁻¹)				¹ H NMR ^c (δ/ppm)		
	C	N	H	Ln	<i>v</i> _{as} (CO ₂)	<i>ν</i> (C–N)	<i>v</i> _s (CO ₂)	<i>ν</i> (C–O) _h	H ₄	H ₅	H ₆
3-hydroxypicolinic acid					1702 s	1608 s	1320 s	1284 vs	7.87	7.79	8.14
[Eu(H ₂ O)(picOH) ₂ (<i>μ</i> -HpicO)]·3H ₂ O 1	32.91 (33.87)	6.85 (6.58)	3.11 (3.16)	23.41 (23.81)	1621 vs <i>1619(1)</i>	1590 vs <i>1596(1)</i>	1344 s <i>1322(1)</i>	1265 s <i>1259(2)</i>	10.0	7.5	11.3
[Tb(H ₂ O)(picOH) ₂ (<i>μ</i> -HpicO)]·3H ₂ O 2	32.12 (33.50)	6.69 (6.51)	3.35 (3.12)	23.39 (24.63)	1623 vs <i>1626(1)</i>	1592 vs <i>1598(2)</i>	1344 s <i>1322(1)</i>	1265 s <i>1259(2)</i>	47	36	57
[Er(H ₂ O)(picOH) ₂ (<i>μ</i> -HpicO)]·3H ₂ O 3	32.45 (33.08)	6.59 (6.43)	3.27 (3.08)	25.66 (25.59)	1625 vs <i>1623(1)</i>	1594 vs <i>1597(1)</i>	1344 s <i>1325(1)</i>	1265 s <i>1259(2)</i>	10.8	6.3	13.0

^a Calculated values in parentheses. ^b Infrared and Raman (in italics) data: vs, very strong; s, strong. ^c Spectra in CD₃SO solution.

ligands having *N,O* chelation mode, while the third proton was found to be bonded to the nitrogen of the pyridine ring (for details see above) of the bridging HpicO⁻ ligand. Several intramolecular hydrogen bonds involving the phenolic OH in picOH⁻ ligands or the protonated pyridinic nitrogen N–H and the corresponding carboxylate in HpicO⁻ were found. The dimensions of these hydrogen bonds are given in Table 3 together with other intermolecular hydrogen bonding interactions.

As described above, in the crystal lattice the HpicO⁻ bridging units act as tridentate ligands and consequently they are the structural motifs that organize the {Eu(H₂O)(picOH)₂(*μ*-picOH)}_{*n*} 1-D polymeric chains. These chains run along the *c* axis and are located around a 2₁ screw crystallographic axis (Figure 1b). Furthermore, a detailed analysis of the crystal structure reveals that 1-D dimensional chains are assembled into a 2-D network through an extensive and complex system of hydrogen bonds between the crystallization waters, the coordinated waters, and the remaining donor atoms of the three 3-hydroxypicolinate ligands, including the bridging one. A view of the crystal-packing diagram of **1**, down the *c* axis, showing the hydrogen bonding interactions is presented in Figure 2 whereas the bond dimensions are listed in Table 3. The most noticeable structural feature of the hydrogen bond pattern is the formation of six-membered centrosymmetric hexagonal supramolecular rings (zone **A** in Figure 2) of oxygen atoms held together by hydrogen bonds. The three unique hydrogen bonds include 2 between coordinated oxygen waters and water bridges (distances for O–H...O 1.89(2), 1.92(4) Å), together with one between adjacent water molecules of 1.99(6) Å. In addition, the aromatic rings of bridging ligands of adjacent 1-D polymeric chains are almost parallel, making a dihedral angle of only 4° and adopting a staggered arrangement

(zone **B** in Figure 2). The distance between the centroids of the π stacking rings is only 3.879 Å. Thus, this geometric arrangement suggests that the crystal structure is also stabilized by face-to-face π stacking interactions.

Vibrational and NMR Spectra. Infrared and Raman spectroscopic data for 3-hydroxypicolinic acid (HpicOH) and its complexes are shown in Table 4, with tentative assignments based on those found in the literature for HpicOH *d*-transition metal complexes.^{13,14} The selected bands of the free ligand, namely the carboxylate asymmetric and symmetric stretches, *v*_{as}(CO₂) and *v*_s(CO₂), and the C–O stretch of the carbon bound to the hydroxyl group, *ν*(C–O)_h, are sensitive to metal coordination as reported for complexes of hydroxybenzoic acids.^{15,16}

In the infrared and Raman spectra, the asymmetric mode *v*_{as}(CO₂) shows shifts (up to 83 cm⁻¹) to a lower wavenumber on coordination when compared to the free ligand (at 1702 cm⁻¹), showing that the ligand is bound to the lanthanide through the carboxylate oxygen. The crystal structure of **1** shows that, in fact, two of the picOH⁻ ligands are bound through *N,O*-chelation, with a carboxylate oxygen coordinated to the lanthanide, while the third ligand shows *O,O*-chelation with the carboxylate group also making a bridge to the nearest lanthanide and thus having both carboxylate oxygens coordinated. The symmetric mode *v*_s(CO₂) shows smaller shifts (up to 24 cm⁻¹) to higher wavenumber on coordination when compared to the free ligand (at 1320 cm⁻¹). Similar shifts were reported for salicylic acid complexes.¹⁶

The pyridine *ν*(C–N) stretch, at 1608 cm⁻¹ for the free ligand, shows shifts up to 18 cm⁻¹, on coordination to the lanthanide ion. These shifts, on both infrared and Raman spectra, show that coordination to the lanthanide ion also involves the nitrogen atom of HpicOH,

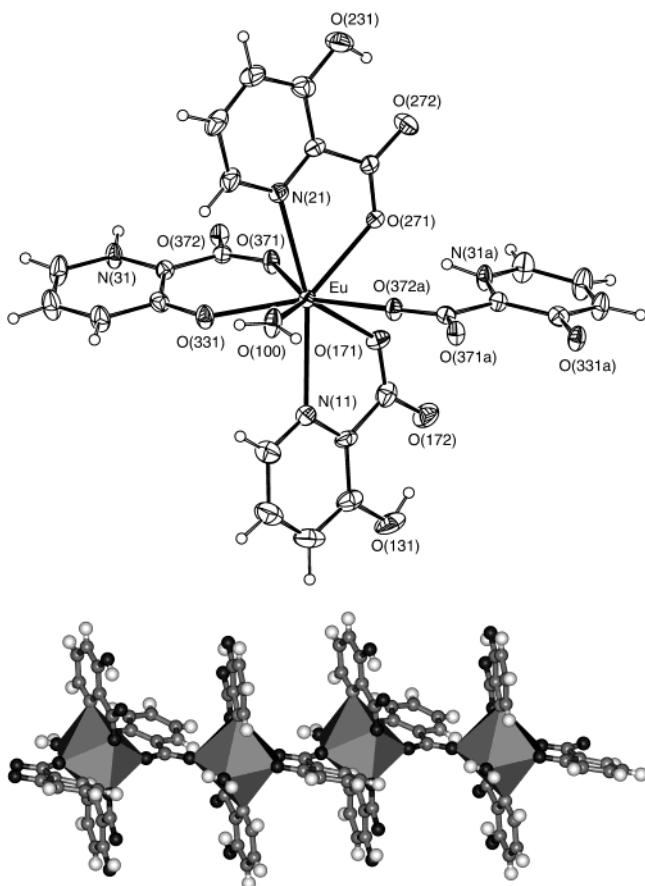


Figure 1. Crystal structure of $[\text{Eu}(\text{H}_2\text{O})(\text{picOH})_2(\mu\text{-HpicO})]\cdot 3\text{H}_2\text{O}$ **1**: (a) ORTEP view of the building unit of **1** showing the atomic connectivities, labeling scheme adopted, and the thermal ellipsoids drawn at 30% of probability level; labels of the carbon atoms are omitted for clarity; and (b) view of the polymeric $\{\text{Eu}(\text{H}_2\text{O})(\text{picOH})_2(\mu\text{-picOH})\}_n$ 1-D chain down the c axis with the Eu^{3+} centers drawn in the polyhedra style.

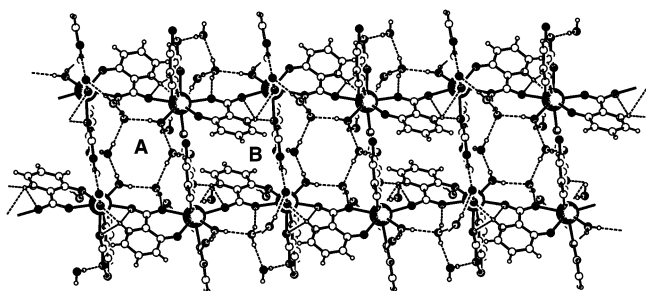
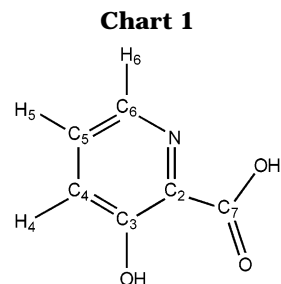


Figure 2. View of the crystal packing diagram of **1** down the c axis showing how the $\{\text{Eu}(\text{H}_2\text{O})(\text{picOH})_2(\mu\text{-picOH})\}_n$ 1-D polymeric chains are assembled by water molecules via hydrogen bond into a 2-D network running along the $[100]$ crystallographic plane.

according to the N,O -chelation of two of the coordinated picOH^- ligands seen in the crystal structure of **1**. A N,O -chelation has also been reported for Ln complexes with picolinic and dipicolinic acids.⁷ Shifts of 19 cm^{-1} shown in the complexes spectra for the bands assigned to the $\nu(\text{C}-\text{O})_h$ stretch (at 1284 cm^{-1} for the hydroxyl group of the free ligand), are possibly due both to the O,O -chelation of one ligand, and to hydrogen bonding to the adjacent carboxylate group in the other two picOH^- ligands bound through N,O -chelation. The infrared spectra of the lanthanide complexes show a very strong absorption in the region $3000\text{--}3500\text{ cm}^{-1}$, assigned to



the stretching vibrations of the $\text{O}-\text{H}$ bonds in (a) the hydroxyl group of the N,O -chelated picOH^- ligand (maximum at 3175 cm^{-1}), (b) the coordinated water molecules (maximum at 3260 cm^{-1}), and (c) the crystallization water molecules (maximum at 3380 cm^{-1}).

The ^1H NMR signals for the $[\text{Ln}(\text{H}_2\text{O})(\text{picOH})_2(\mu\text{-HpicO})]\cdot 3\text{H}_2\text{O}$ complexes are broad, and relative intensities cannot be discussed. All the Ln compounds reported here show a set of three signals located close to each other (see Chart 1 for labeling and Table 4 for tentative assignments). These resonances are assigned to the three protons of the pyridine ring. Strong shifts can be induced by the lanthanide ion, in particular in the case of the $\text{Tb}(\text{III})$ complex.

The X-ray powder diffraction patterns for complexes **1**, **2**, and **3** show that these compounds are isostructural. This, together with the vibrational spectroscopy data, confirms the same type of coordination for all the Ln complexes reported here.

Photoluminescence Spectra. Figure 3A and B show the room temperature (RT) photoluminescence (PL) spectra for the HpicOH ligand, Tb^{3+} , and Eu^{3+} complexes. The sharp lines are assigned to transition between the first excited state ($^5\text{D}_4$ and $^5\text{D}_0$, for Tb^{3+} and Eu^{3+} , respectively) and the ground multiplet, $^7\text{F}_{6-3}$ and $^7\text{F}_{0-4}$, for Tb^{3+} and Eu^{3+} , respectively. The large broad band in the green-blue spectral region is also observed in the PL spectrum of the HpicOH ligand, peaking around 418 nm (Figure 3A), and may be assigned to the emission from $\pi\pi^*$ states of the chelate ring, as reported for terpyridine,²⁹ for instance. When the lanthanide ions are coordinated the emission energy of the ligand broad band is altered. In the case of the Tb^{3+} complex, its maximum intensity position shifts from 418 to 420 nm . This indicates an effective interaction between the terbium ion and the picOH ligand. Moreover, the differences in the relative intensity of this broad band with respect to the Tb^{3+} and Eu^{3+} lines (Figure 3A and B) indicate that energy transfer occurs between the ligand and the lanthanide ions. As no emission intensity from the ligand could be detected in the Eu^{3+} complex, the emission spectrum displays only the intra- $4f^6$ $^5\text{D}_0 \rightarrow ^7\text{F}_{0-4}$ transitions (Figure 3B); this energy transfer process seems to be very efficient for that compound. The inset of Figure 3B illustrates this ligand-to-metal energy transfer for the Eu^{3+} complex. Besides the intra- $4f^6$ $^7\text{F}_0 \rightarrow ^5\text{L}_6$, $^5\text{D}_{2,1}$ transitions, the photoluminescence excitation spectrum displays a very large broad band between 320 and 400 nm associated with the HpicOH ligand.

The lifetime of the Eu^{3+} first excited state, $\tau_{\text{exp}}(^5\text{D}_0)$, was detected at 614 nm (the more intense Eu^{3+} emission

(29) Fink, D. W.; Ohnesorge, W. E. *J. Phys. Chem.* **1970**, *74*, 72.

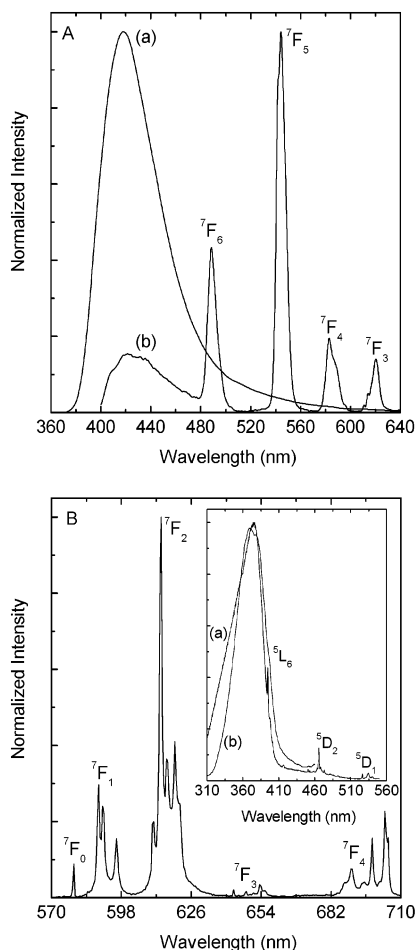


Figure 3. Room-temperature PL spectra (excited at 325 nm) for A: HpicOH ligand, (a) and $[\text{Tb}(\text{H}_2\text{O})(\text{picOH})_2(\mu\text{-HpicO})]\cdot 3\text{H}_2\text{O}$, (b). B: $[\text{Eu}(\text{H}_2\text{O})(\text{picOH})_2(\mu\text{-HpicO})]\cdot 3\text{H}_2\text{O}$. The sharp lines are assigned to the ${}^5\text{D}_4 \rightarrow {}^7\text{F}_{6,5,4,3}$ (Tb^{3+}) and ${}^5\text{D}_0 \rightarrow {}^7\text{F}_{0,1,2,3,4}$ (Eu^{3+}) transitions, respectively. The inset shows the excitation spectra recorded at RT for HpicOH ligand, (a) and $[\text{Eu}(\text{H}_2\text{O})(\text{picOH})_2(\mu\text{-HpicO})]\cdot 3\text{H}_2\text{O}$ (b), monitored at 420 and 614 nm, respectively.

line) with an excitation wavelength of 395 nm. The decay profile is well reproduced by a single-exponential that reveals a lifetime of 0.481 ± 0.002 ms.

We can estimate the efficiency, q , of the ${}^5\text{D}_0$ Eu^{3+} excited state. Assuming that only nonradiative and radiative processes are essentially involved in the depopulation of the ${}^5\text{D}_0$ state, q can be defined as follows:

$$q = \frac{k_r}{k_r + k_{nr}} \quad (1)$$

where k_r and k_{nr} are the radiative and the nonradiative transition probabilities, respectively.

The emission intensity, I , taken as the integrated intensity S of the emission curves, for the ${}^5\text{D}_0 \rightarrow {}^7\text{F}_{0-4}$ transitions, is expressed by

$$I_{i-j} = \hbar \omega_{i-j} A_{i-j} N_i \equiv S_{i-j} \quad (2)$$

where i and j represent the initial (${}^5\text{D}_0$) and final levels (${}^7\text{F}_{0-4}$), respectively, $\hbar \omega_{i-j}$ is the transition energy, A_{i-j} corresponds to the Einstein's coefficient of spontaneous emission, and N_i is the population of the ${}^5\text{D}_0$ emitting

level.^{30,31} The radiative contribution may be calculated from the relative intensities of the ${}^5\text{D}_0 \rightarrow {}^7\text{F}_{0-4}$. The branching ratio for the ${}^5\text{D}_0 \rightarrow {}^7\text{F}_{5,6}$ transitions must be neglected as they are not observed experimentally. Therefore, we can ignore their influence in the depopulation of the ${}^5\text{D}_0$ excited state. Because the ${}^5\text{D}_0 \rightarrow {}^7\text{F}_1$ transition can be considered as a reference, due to its dipolar magnetic nature k_r can be calculated as follows:

$$k_r = A_{0-1} \frac{\hbar \omega_{0-1} \sum_{J=0}^4 \frac{S_{0-J}}{\hbar \omega_{0-J}}}{S_{0-1}} \quad (3)$$

where A_{0-1} is the Einstein's coefficient of spontaneous emission between the ${}^5\text{D}_0$ and the ${}^7\text{F}_1$ Stark levels. The ${}^5\text{D}_0 \rightarrow {}^7\text{F}_1$ transition does not depend on the local ligand field seen by Eu^{3+} ions and thus may be used as a reference for the whole spectrum, $A_{0-1} \approx 50 \text{ s}^{-1}$.³² We found a q value of $\approx 13.5\%$ for the Eu^{3+} emission in the $[\text{Eu}(\text{H}_2\text{O})(\text{picOH})_2(\mu\text{-HpicO})]\cdot 3\text{H}_2\text{O}$ complex. The corresponding value of k_r is 0.281 ms^{-1} .

[Ln(H₂O)(picOH)₂(μ-HpicO)]·3H₂O/SiO₂ Nanocomposite Materials. It was found that complex **1** can be dispersed within amorphous silica. There is a particular interest in making this type of nanocomposite because it will allow cast pieces of a luminescent material to be fabricated using the sol-gel method. The preparation of such a composite involves the synthesis of colloidal SiO₂ in the presence of the Eu(III) complex **1**, using an adaptation of the Stöber method.²¹ Figure 4 shows the SEM images of SiO₂ particles prepared in the absence (a) or in the presence (b) of complex **1** (Eu/SiO₂ composite **B**). As expected, this method led to well-defined spherical SiO₂ sub-micrometric particles in both cases, although a slight agglomeration of the particles occurred when the complex was present. The presence of the complex clearly has an influence on the particles size distribution; with the average diameter of the particles decreasing from $472 \pm 27 \text{ nm}$ to $127 \pm 9 \text{ nm}$. It is well-known that colloidal SiO₂ forms three-dimensional networks involving chemical reactions at the surface.³³ Several experimental parameters have been reported to have a strong influence on the type of SiO₂ obtained and in particular on its morphological properties.³³ Thus, the presence of chemical species which may interact with the SiO₂ surface can lead to noticeable morphological modifications. The difference observed on the SiO₂ particles size distribution (Figure 4) can be related to particle growth inhibition due to the presence of the complex at the SiO₂ surfaces. Although complex **1** is very soluble in DMSO, which was used in this preparation, there is also the possibility that such complex species act as nucleation centers for the SiO₂ growth, therefore increasing the total number of particles and leading to a decrease in the average diameter and standard deviation. The infrared spectra of the SiO₂ particles prepared in the presence of the complex **1** (both Eu/SiO₂ composites **A** and **B**) show

(30) Malta, O. L.; Couto dos Santos, M. A.; Thompson, L. C.; Ito, N. K. *J. Lumin.* **1996**, *69*, 77.

(31) Malta, O. L.; Brito, H. F.; Menezes, J. F. S.; Gonçalves e Silva, F. R.; Alves, S., Jr.; Farias, F. S., Jr.; Andrade, A. V. M. *J. Lumin.* **1997**, *75*, 255.

(32) Hazenkamp, M. F.; Blasse, G. *Chem. Mater.* **1990**, *2*, 105.

(33) Iler, R. K. *The Chemistry of Silica*; Wiley-Interscience: New York, 1979.

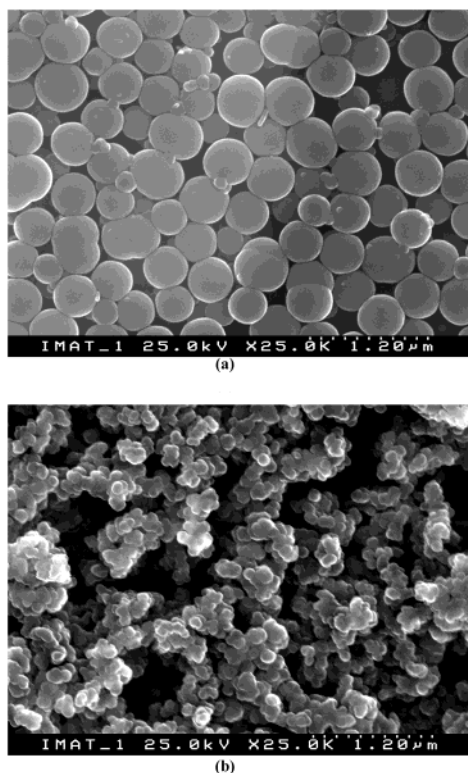


Figure 4. SEM images of SiO₂ particles prepared in the absence (a) or in the presence (b) of the [Eu(H₂O)(picOH)₂(μ -HpicO)]·3H₂O/SiO₂ composite B.

bands at 1637 and 1593 cm⁻¹, assigned to the $\nu_{as}(\text{CO}_2)$ and $\nu(\text{C}-\text{N})$ modes of **1** (Table 4); other characteristic bands of this complex are also seen at 1411 and 1467 cm⁻¹. The bands assigned to the Eu(III) complex **1** in the infrared spectrum of the Eu/SiO₂ composite **A** show a stronger intensity than those observed in the composite **B** spectrum, which suggests a less amount of complex in **B** possibly due to the treatment with NH₄OH used in its preparation. The hydroxyl stretching region at 3500–3700 cm⁻¹ and the region at 1260–1290 cm⁻¹ for the $\nu(\text{C}-\text{O})_h$ modes, are dominated by the silica strong absorption bands.

The [Eu(H₂O)(picOH)₂(μ -HpicO)]·3H₂O/SiO₂ particles (Eu/SiO₂ composite **A**) formed a rigid gel on standing in the reaction vessel for long times. This is due to the formation of a polymeric network following condensation reactions at the silica surfaces; finally, a solid monolith was obtained by slow evaporation of the solvent from the gel. Figure 5 displays the PL spectrum of this monolith, herein referred as the Eu/SiO₂ composite **A**. A series of intra-4f⁶ lines, assigned to the $^5\text{D}_0 \rightarrow ^7\text{F}_{0-4}$ transitions, is observed, together with the presence of the ligand band, peaking around 420 nm. The ligand emission, although with lower relative intensity, with respect to the ion lines, when compared to the spectra of the Tb³⁺ complex (Figure 3), suggests that in the composite **A** the ligand-to-metal energy transfer is less efficient than that in [Eu(H₂O)(picOH)₂(μ -HpicO)]·3H₂O.

When we compare the emission spectrum of the composite **A** with the one characteristic of the precursor complex (Figures 3b and 5), changes are observed in the energy, maximum splitting, and profile of the $^5\text{D}_0 \rightarrow ^7\text{F}_{0-4}$ transitions. The energy of the $^5\text{D}_0 \rightarrow ^7\text{F}_0$ line and its full width at half-maximum (fwhm), for instance,

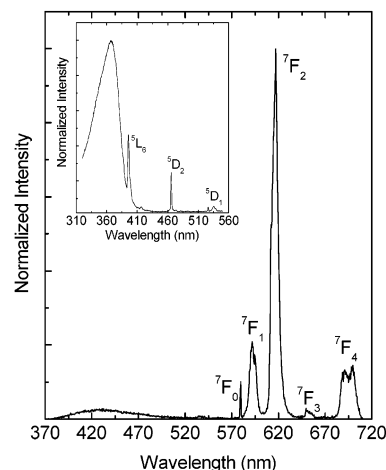


Figure 5. Room-temperature PL spectra (excited at 325 nm) for the [Eu(H₂O)(picOH)₂(μ -HpicO)]·3H₂O/SiO₂ nanocomposite **A**. The sharp lines correspond to the $^5\text{D}_0 \rightarrow ^7\text{F}_{0,1,2,3,4}$ transitions, and the large broad band (less intense relative to the intra-4f⁶ lines) is ascribed to the ligands emission. The inset shows the corresponding RT excitation spectrum, monitored at 617 nm.

increase for the Eu³⁺-based composite **A**, from 17251.39 ± 0.04 to 17259.23 ± 0.10 cm⁻¹ and from 3.96 ± 0.07 to 25.75 ± 0.24 cm⁻¹, respectively. Moreover, the local-field splitting of the $^5\text{D}_0 \rightarrow ^7\text{F}_{1,2}$ transitions in three and five Stark components, respectively, is much more evident in the [Eu(H₂O)(picOH)₂(μ -HpicO)]·3H₂O complex. However, the number of Stark components detected for the $^5\text{D}_0 \rightarrow ^7\text{F}_{1-4}$ transitions in both spectra indicate that the Eu³⁺ ions occupy a very low site symmetry without inversion center, according to the high intensity of the $^5\text{D}_0 \rightarrow ^7\text{F}_2$ transition.

The $^5\text{D}_0$ lifetime was measured around the Eu³⁺ more intense line (616.9 nm) with an excitation wavelength of 395 nm, and the decay profile is also well reproduced by a single-exponential revealing a lifetime of 0.525 ± 0.006 ms. The radiative transition probability for the Eu³⁺-based composite **A** also increases, relative to the precursor complex, and, therefore, a greater efficiency of the $^5\text{D}_0$ Eu³⁺ excited state is found for the composite, $q \approx 20\%$ (the corresponding value of k_r is 0.396 ms⁻¹). We should note that this increase in the $^5\text{D}_0$ emission efficiency is achieved despite the less efficient ligand-to-metal energy transfer process, as stated above.

All the photoluminescent results confirm the presence of the Eu³⁺ complex in the final SiO₂ material and demonstrate the potential of the chemical method reported here to yield high luminescent composites. Moreover, the differences on the energy, profile, and fwhm of the $^5\text{D}_0 \rightarrow ^7\text{F}_{0-4}$ transitions, and on the $^5\text{D}_0$ lifetime between the two materials, clearly indicate modifications in the Eu³⁺ local environment as the [Eu(H₂O)(picOH)₂(μ -HpicO)]·3H₂O complex is dispersed within the silica gel. This conclusion will be quantitatively stressed by calculating the experimental intensity parameters Ω_2 and Ω_4 .

Usually the experimental intensity parameters are obtained from absorption data. However, in the case of Eu³⁺ the pure magnetic dipolar character displayed by the $^5\text{D}_0 \rightarrow ^7\text{F}_1$ transition allows the determination of the intensity parameters from emission spectra. In addition, the electric dipolar $^5\text{D}_0 \rightarrow ^7\text{F}_{2,4,6}$ transitions

depend only on the $U^{(2)}$, $U^{(4)}$, and $U^{(6)}$ reduced matrix elements, respectively, which allows the evaluation of the experimental intensity $\Omega_{2,4,6}$ parameters directly from emission data.^{30,31,34} On the basis of the luminescence spectra for the $[\text{Eu}(\text{H}_2\text{O})(\text{picOH})_2(\mu\text{-HpicO})]\cdot 3\text{H}_2\text{O}$ and $[\text{Eu}(\text{H}_2\text{O})(\text{picOH})_2(\mu\text{-HpicO})]\cdot 3\text{H}_2\text{O}/\text{SiO}_2$ (Figure 5) the experimental intensity parameters Ω_2 and Ω_4 were determined using the ${}^5\text{D}_0 \rightarrow {}^7\text{F}_2$ and ${}^5\text{D}_0 \rightarrow {}^7\text{F}_4$ transitions, respectively. The $A_i \rightarrow j$ Einstein coefficient is given by the following:^{30,31,34}

$$A_{i \rightarrow j} = \frac{4e^2\omega^3}{3\hbar c^3} \frac{1}{2J+1} \chi \sum_{\lambda} \Omega_{\lambda} \langle {}^7F_j || U^{(\lambda)} || {}^5D_0 \rangle^2 \quad (4)$$

where ω is the frequency of the transition and $\chi = n_0(n_0^2 + 2)^2/9$, a Lorentz local field correction for the index of refraction n_0 of the medium. The reduced matrix elements in eq 4 were taken from Carnall et al.³⁵ and an average index of refraction equal to 1.5 was used.^{30,31,34} The Ω_6 intensity parameter was not determined because the ${}^5\text{D}_0 \rightarrow {}^7\text{F}_6$ transition could not be experimentally detected. This stresses, therefore, that Ω_6 is not important here. The obtained values (in units of 10^{-20} cm^2) are 14.1 and 20.5, Ω_2 , and 7.8 and 13.0, Ω_4 , for $[\text{Eu}(\text{H}_2\text{O})(\text{picOH})_2(\mu\text{-HpicO})]\cdot 3\text{H}_2\text{O}$ and $[\text{Eu}(\text{H}_2\text{O})(\text{picOH})_2(\mu\text{-HpicO})]\cdot 3\text{H}_2\text{O}/\text{SiO}_2$, respectively.

The interpretation of the physical meaning of the phenomenological Judd-Ofelt intensity parameters still remains a controversial matter for discussion. There have been many attempts in the literature to relate the observed variations with some specific ligand field effects.³⁶ Ω_2 variations are usually related to the degree of covalency in the lanthanide–first coordination shell interaction.^{30,31,36–38} In the sense of the dynamic coupling contribution to the total intensity,³⁸ the polarization of the ligand field induces stronger lanthanide–ligand bonds and an increase in electric dipolar transitions for noncentrosymmetric ligand fields. On the other hand, $\Omega_{4,6}$ parameters have been related together to bulk properties of the lanthanide-based hosts (viscosity, for instance).^{30,31,36,37} There is no theoretical prediction for this sensibility to macroscopic properties, but empirical variations seem to suggest some kind of relationship.

Comparing the values found for the precursor complex and for the Eu^{3+} -based composite **A**, we note an increase in both values (by a factor of 1.5) as the complex is dispersed within the silica network. This seems to point out that there is an appreciable variation both on the polarizability of the first coordination shell for the composite and that the steric effects are more significant in this compound, as expected if we are explicitly assuming the Eu^{3+} coordination to the surface of the spherical SiO_2 sub-micrometric particles via silanol groups.

Next, a possible Eu^{3+} -first coordination shell in the Eu/SiO_2 composite **A** is discussed using the energy shift of the ${}^5\text{D}_0 \rightarrow {}^7\text{F}_0$ transition, with respect to the energy calculated for gaseous Eu^{3+} , and the phenomenological evaluation of the number of water molecules coordinated to the metal ion, n_w .

The red-shift observed in the ${}^5\text{D}_0 \rightarrow {}^7\text{F}_0$ energy, with respect to the energy calculated for gaseous Eu^{3+} (17374 cm^{-1}),^{34,39,40} is related to the nature of the first coordination shell through the following phenomenological equation:

$$\Delta E \equiv E({}^5D_0 \rightarrow {}^7F_0)_{\text{complex}} - E({}^5D_0 \rightarrow {}^7F_0)_{\text{gaseous}} = C_N(n_1\delta_1 + \dots + n_j\delta_j) \quad (5)$$

in which C_N is an adjustable coefficient associated with the total number of Eu^{3+} first-neighbors, n_j is the number of type j atoms in the first coordination shell, and δ_j is an adjusted parameter which measures the tendency of an atom to bond covalently to the Eu^{3+} cation.³⁹ Attending to the X-ray data for complex **1**, a Eu^{3+} first coordination shell composed of four charged carboxylate oxygens, OT, two amine nitrogen atoms, NT, one water molecule, OW, and one hydroxyl oxygen, OH, we found a ${}^5\text{D}_0 \rightarrow {}^7\text{F}_0$ energy shift of $-121.9 \pm 3 \text{ cm}^{-1}$, very close to the experimental value of $-122.2 \pm 0.7 \text{ cm}^{-1}$. The corresponding experimental energy shift found for the Eu^{3+} -based composite **A** is $-114.8 \pm 0.7 \text{ cm}^{-1}$.

Horrocks and Sudnick suggested that the number of water molecules coordinated to the metal ion could be evaluated according to the empirical formula⁴¹

$$n_w = 1.05(k_{\text{exp}} - k_r) \quad (6)$$

where k_{exp} is the total transition probability, $k_{\text{exp}} = 1/\tau_{\text{exp}} = k_r + k_{\text{nr}}$. We can use k_r substituted for the value obtained in D_2O , as originally proposed.⁴¹ We found that the number of water molecules belonging to the Eu^{3+} first coordination shell is similar for both the complex and the nanocomposite, 1.9 ± 0.5 and 1.6 ± 0.5 , respectively. Therefore, on the basis of this result and the energy shift of the ${}^5\text{D}_0 \rightarrow {}^7\text{F}_0$ transition, we suggest that in the nanocomposite the complex is bound to the silica surface via silanol groups, possibly displacing one bridging carboxylate group from the Eu^{3+} first coordination shell. The predicted value of eq 5 for a Eu^{3+} first coordination shell involving 3 OT, 2 NT, 1 OW, and 2 OH is $-116.0 \pm 3.0 \text{ cm}^{-1}$, very close to the experimental value.

Conclusions

Novel luminescent composite materials have been prepared by a sol–gel method. The materials consist of a SiO_2 matrix that hosts an anchored $\text{Eu}(\text{III})$ complex with coordinated 3-hydroxypicolinate ligands, $[\text{Eu}(\text{H}_2\text{O})(\text{picOH})_2(\mu\text{-HpicO})]\cdot 3\text{H}_2\text{O}$ **1**. The X-ray crystal structure of **1** shows two picOH^- ligands coordinated by N, O -

(34) Carlos, L. D.; Messaddeq, Y.; Brito, H. F.; Sá-Ferreira, R. A.; de Zea Bermudez, V.; Ribeiro, S. J. L. *Adv. Mater.* **2000**, *12*, 594.

(35) Carnall, W. T.; Crosswhite, H.; Crosswhite, H. M. *Energy Structure and Transition Probabilities of the Trivalent Lanthanides in LaF₃*; Argonne National Laboratory Report, unnumbered; 1977.

(36) Reisfeld, R.; Jørgensen, C. K. In *Handbook on the Physics and Chemistry of Rare Earths*; Gschneidner, K. A., Eyring, L., Eds.; North-Holland: Amsterdam, The Netherlands, 1987; Vol. 9, Ch. 58, and references therein.

(37) Oomen, E. W. J. L.; van Dongen, A. M. A. *J. Non-Cryst. Solids* **1989**, *111*, 205.

(38) Judd, B. R. *J. Chem. Phys.* **1979**, *70*, 4830.

(39) Horrocks, W. D., Jr.; Sudnick, W. D. R. *Acc. Chem. Res.* **1981**, *12*, 384.

(40) Frey, S. T.; Horrocks, W. D. W., Jr. *Inorg. Chim. Acta* **1995**, *229*, 383.

(41) Carlos, L. D.; Sá-Ferreira, R. A.; de Zea Bermudez, V.; Molina, C.; Bueno, L. A.; Ribeiro, S. J. L. *Phys. Rev. B* **1999**, *60*, 10042.

chelation, and the third ligand bound through *O,O*-chelation with the carboxylate group making a bridge to the nearest lanthanide, one water molecule and a hydroxyl group completes the Eu(III) first coordination shell; the Tb(III) and Er(III) complexes are isostructural as shown by X-ray powder diffraction and the spectroscopy results. The Eu(III) complex **1** was dispersed within a silica matrix by the in situ preparation of silica nanoparticles using the Stöber method. The photoluminescent features of the composite, namely the experimental 5D_0 lifetime, the energy of the $^5D_0 \rightarrow ^7F_0$ transition, and the calculated values for the experimental intensity parameters, strongly suggest that the Eu^{3+} are coordinated to the surface of the nanoparticles. To better understand the composite's properties, the preparation of a series of SiO_2 nanocomposites incorporating

other Ln complexes with aromatic ambidentate ligands is in progress.

Acknowledgment. P.S.-S. thanks the University of Aveiro for a Ph.D. research grant. R.A.S.F. thanks the Fundação para a Ciência e Tecnologia (FCT) for grant PRAXIS/BD/18404/98. We thank the FCT for financial support (grant contracts POCTI/35378/QUI/00 and POCTI/33653/CTM/00) as supported by FEDER. We thank the EPSRC and the University of Reading for funds for the Image Plate system.

Supporting Information Available: Crystallographic data (CIF). This material is available free of charge via the Internet at <http://pubs.acs.org>.

CM021188J